Supporting information

Ferromagnetism above Room Temperature in Janus Fe_2X (X = S, Se) Monolayers

Fanjunjie Han[a] and Guochun Yang[a,b,*]

[a]*Centre for Advanced Optoelectronic Functional Materials Research and Key Laboratory for UV Light-Emitting Materials and Technology of Ministry of Education, Northeast Normal University, Changchun 130024, China*

[b]*State Key Laboratory of Metastable Materials Science & Technology and Key Laboratory for Microstructural Material Physics of Hebei Province, School of Science, Yanshan University, Qinhuangdao 066004, China*

E-mail: yanggc468@nenu.edu.cn

Index **page**

1. Computational details 3

2. Structural parameters of the Janus Fe_2X (X = S, Se) monolayers 6

3. Basic building block of the Janus Fe_2X monolayers and phonon dispersive curves for Janus Fe_2Se monolayer 6

4. ELF of different faces for the Janus Fe_2X monolayers..7

5. Crystal orbital Hamilton population (COHP) curves of the Janus Fe_2X monolayers 7

6. AIMDs, Young's modulus $Y(\theta)$, and Poisson's ratio $\nu(\theta)$ for the Janus Fe_2X monolayers 8

7. Convex hull of the Janus Fe_2X monolayers...9

8. Elastic constants of the Janus Fe_2S and Fe_2Se monolayers 10

9. Relative energies of different magnetic configurations for the Janus Fe_2Se monolayer 10

10. Spin-polarized charge density and differential charge density of the Janus Fe_2Se monolayer 10

11. Bader charge of the Janus Fe_2S and Fe_2Se monolayers...10

12. Spin-polarized electronic band structure and PDOS of the Janus Fe_2Se monolayer.....................11

13. PDOS with spin-down state of the Janus Fe_2S monolayer 11

14. Coupling interaction strength of interlayer Fe ions with the increasing distance..........................11

15. Magnetic properties for the Janus Fe_2Se monolayer and angular-dependent MAE of the Janus Fe_2X monolayers..12

16. Atomic structures of the point defects in the Janus Fe_2X monolayers 12

17. Formation energies of the point defects of the Janus Fe_2X monolayers..13

18. Magnetic properties for the Janus Fe_2X monolayers with Fe-I_X defect..13

19. T_Cs and MAEs of the Janus Fe_2Se monolayer under biaxial strains...14

20. Phonon dispersive curves for the TS of Janus Fe_2S monolayer 14

21. Structural information..14

22. References..15

Computational Details

The particle swarm optimization (PSO) method within the evolutionary algorithm as implemented in the Crystal structure AnaLYsis by Particle Swarm Optimization (CALYPSO) code[1,2] was applied to find new structures of Fe_2X (X = S, Se) monolayers. Unit cells containing 1, and 2 formula units (f.u.) were considered. In the first step, random structures with certain symmetry are constructed in which atomic coordinates are generated by the crystallographic symmetry operations. Local optimizations using the VASP code[3] were done with the conjugate gradients method and stopped when Gibbs free energy changes became smaller than 1×10^{-5} eV per cell. After processing the first-generation structures, 60% of them with lowest Gibbs free energies are selected to construct the next generation structures by PSO. 40% of the structures in the new generation are randomly generated. A structure fingerprinting technique of bond characterization matrix is applied to the generated structures, so that identical structures are strictly forbidden. These procedures significantly enhance the diversity of the structures, which is crucial for structural global search efficiency. In most cases, structural searching simulations for each calculation were stopped after generating 1000~ 1200 structures (e.g., about 20 ~ 30 generations).

The local structural relaxations and electronic property calculations were performed in the framework of the density functional theory (DFT)[4] within the generalized gradient approximation (GGA)[5] as implemented in the VASP code. The projector augmented wave (PAW) method is used to treat the ion-electron interaction, in which the valence electrons of each atom are Fe: $3d^7 4s^1$, S: $3s^2 3p^4$, Se: $4s^2 4p^4$.

We calculated the cohesive energy of the Janus Fe_2X (X = S, Se) monolayer by using the following expression:

$$E_{coh} = (2E_{Fe} + E_X - E_{Fe_2X})/3$$

where E_{Fe}, E_{X} and E_{Fe_2X} are the total energies of a single Fe atom, S/Se atom and the Janus Fe_2X monolayers, respectively.

The Young's modulus $Y(\theta)$ and Poisson's ratio $v(\theta)$ along any direction θ (θ is the angle with respect to the positive x-direction) are defined as

$$Y(\theta) = \frac{C_{11}C_{22} - {C_{12}}^2}{C_{11}s^4 + C_{22}c^4 + (\frac{C_{11}C_{22} - {C_{12}}^2}{C_{66}} - 2C_{12})c^2s^2}$$

$$v(\theta) = \frac{C_{12}(c^4 + s^4) - (C_{11} + C_{22} - \frac{C_{11}C_{22} - {C_{12}}^2}{C_{66}})c^2s^2}{C_{11}s^4 + C_{22}c^4 + (\frac{C_{11}C_{22} - {C_{12}}^2}{C_{66}} - 2C_{12})c^2s^2}$$

were c = $\cos\theta$ and s = $\sin\theta$.

Based on the Heisenberg model, the different magnetic configurations for the Janus Fe_2X monolayers are given by the following expressions:

$$E_{FM} = E_0 - 3J_1\vec{S}^2 - 6J_2\vec{S}^2 - D\vec{S}^2,$$

$$E_{Neel-AFM} = E_0 + 3J_1\vec{S}^2 - 6J_2\vec{S}^2 - D\vec{S}^2,$$

$$E_{Stripy-AFM} = E_0 + J_1\vec{S}^2 + 2J_2\vec{S}^2 - D\vec{S}^2,$$

$$E_{Zigzag-AFM} = E_0 - J_1\vec{S}^2 + 2J_2\vec{S}^2 - D\vec{S}^2.$$

where E_0 is the energy without magnetic order, and S is set to 1.5. Hence, we can estimate the magnetic coupling parameters J_1 and J_2 by solving these four equations:

$$J_1 = \frac{E_{Neel-AFM} - E_{FM}}{6\vec{S}^2}$$

$$J_2 = \frac{2E_{Zigzag-AFM} - E_{FM} - E_{Stripy-AFM}}{8\vec{S}^2}$$

Under thermodynamic equilibrium, the quantity of primary interest in governing the relative stability of defects is their formation energy (E_{form}). The formation energy takes the form

$$E_{form} = (E_{defect} - E_{host} \pm N\mu)$$

where E_{defect} and E_{host} are the total energy of the Janus Fe_2X monolayers with and without point defect, respectively. N is the number of the surplus (-) or poor (+) atoms compared with the perfect Fe_2X, and μ is the corresponding chemical potential.

Different magnetic configurations for the Janus Fe_2X monolayers in 2×2×1 supercell with the Fe-

I_X defect are given by the following expressions:

$$E_{FM} = E_0 - 9J_1\vec{S}^2 - 18J_2\vec{S}^2 - D\vec{S}^2,$$

$$E_{Neel-AFM} = E_0 + 9J_1\vec{S}^2 - 18J_2\vec{S}^2 - D\vec{S}^2,$$

$$E_{Stripy-AFM} = E_0 + 3J_1\vec{S}^2 + 6J_2\vec{S}^2 - D\vec{S}^2,$$

$$E_{Zigzag-AFM} = E_0 - 3J_1\vec{S}^2 + 6J_2\vec{S}^2 - D\vec{S}^2.$$

Here, the magnetic coupling parameters J_1 and J_2 of the Janus Fe_2X monolayers with point defect by solving these four equations:

$$J_1 = \frac{E_{Neel-AFM} - E_{FM}}{18\vec{S}^2}$$

$$J_2 = \frac{2E_{Zigzag-AFM} - E_{FM} - E_{Stripy-AFM}}{24\vec{S}^2}$$

The Curie temperature was calculated by the Monte Carlo method with the Metropolis algorithm based on the 2D anisotropy Heisenberg model. All of them were implemented in MCSOLVER.[6]

Supporting Figures and Tables

Table S1. Structural parameters of the predicted Janus Fe_2X (X = S, Se) monolayers: space group (SG), lattice constants *a* and *b*, layer thickness *h*, bond lengths of Fe_I-Fe_{II} d_1, Fe_I-Fe_I /(Fe_{II}-Fe_{II}) d_2, Fe_{II}-S/Se d_3, and Fe_I-S/Se d_4.

	SG	*a/b* (Å)	*h* (Å)	d_1 (Å)	d_2 (Å)	d_3 (Å)	d_4 (Å)
Fe_2S	*P*3*m*1	2.90	3.36	2.48	2.90	2.27	3.75
Fe_2Se	*P*3*m*1	2.97	3.52	2.47	2.97	2.45	3.91

The relaxed lattice constants are $a = b = 2.90/2.97$ Å for the Janus Fe_2S/Fe_2Se monolayers. The interlayer distance of Fe atoms is 2.48 Å for Fe_2S and 2.47 Å for Fe_2Se, respectively, much smaller than the intralayer ones and comparable to the Fe-Fe bond in 2D Fe2Si (2.43 Å)[7] and bulk Fe with *Im*3*m* symmetry (2.48 Å).[8] Meanwhile, the optimized Fe_{II}-S and Fe_{II}-Se bonds lengths of 2.27 and 2.45 Å, respectively, which are slightly larger than the Fe-S bond (2.22 Å) in H-FeS_2 and the Fe-Se bond (2.35 Å) in H-$FeSe_2$.[9]

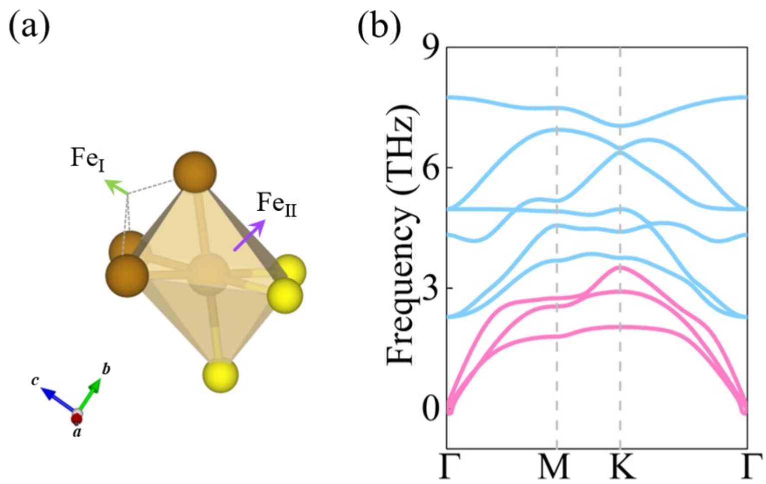

Figure S1. (a) Octahedral-like building block. (b) Phonon dispersive curves of the Janus Fe_2Se monolayer.

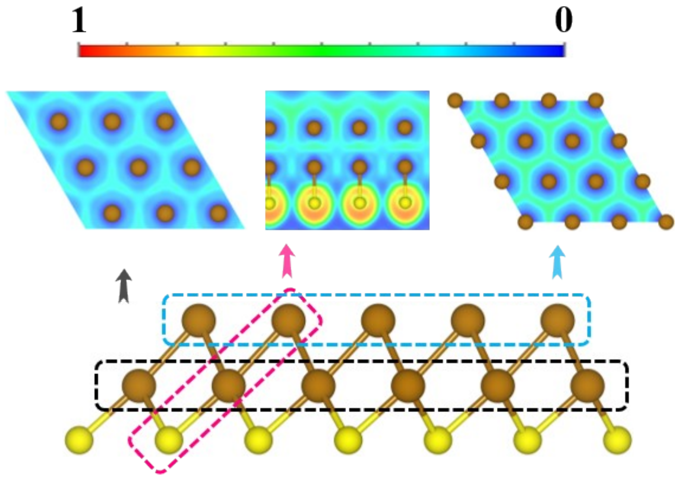

Figure S2. ELF maps of different faces in the Janus Fe_2X (X = S, Se) monolayers.

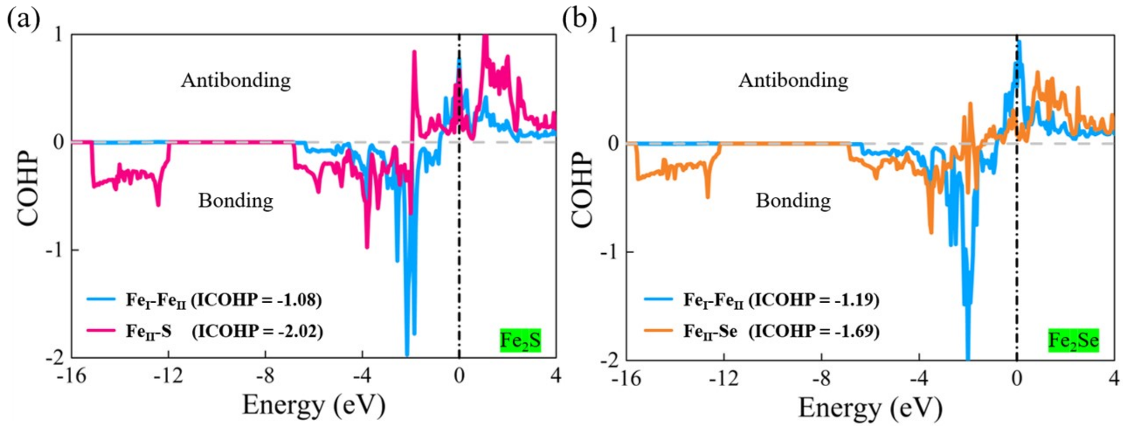

Figure S3. Crystal orbital Hamilton population (COHP) curves of the adjacent Fe_I-Fe_{II} and Fe_{II}-S/Se pairs in the Janus (a) Fe_2S and (b) Fe_2Se monolayers.

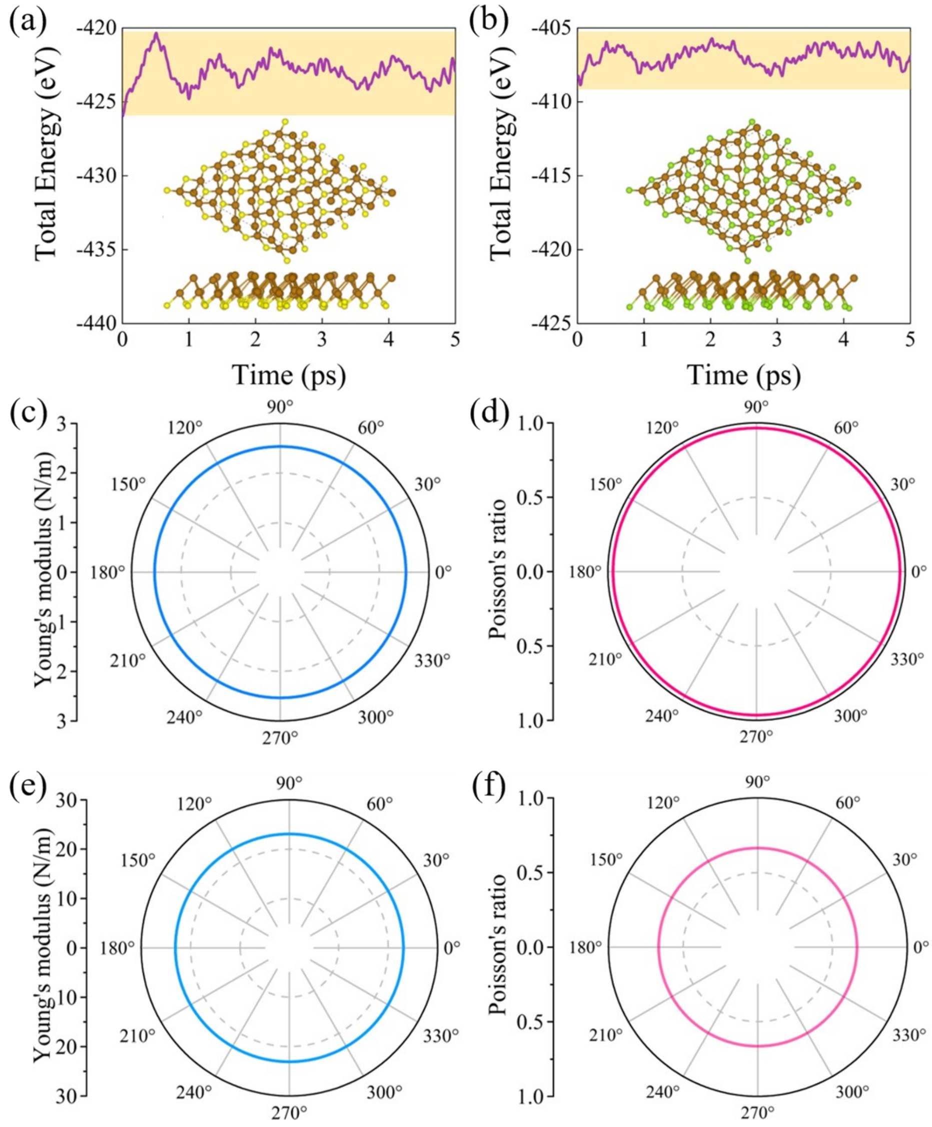

Figure S4. Total energies and the snapshots of the final frames for the Janus (a) Fe_2S and (b) Fe_2Se monolayers. Orientation-dependent in-plane Young's modulus $Y(\theta)$ and Poisson's ratio $\nu(\theta)$ of the Janus (c, d) Fe_2S and (e, f) Fe_2Se monolayers, respectively.

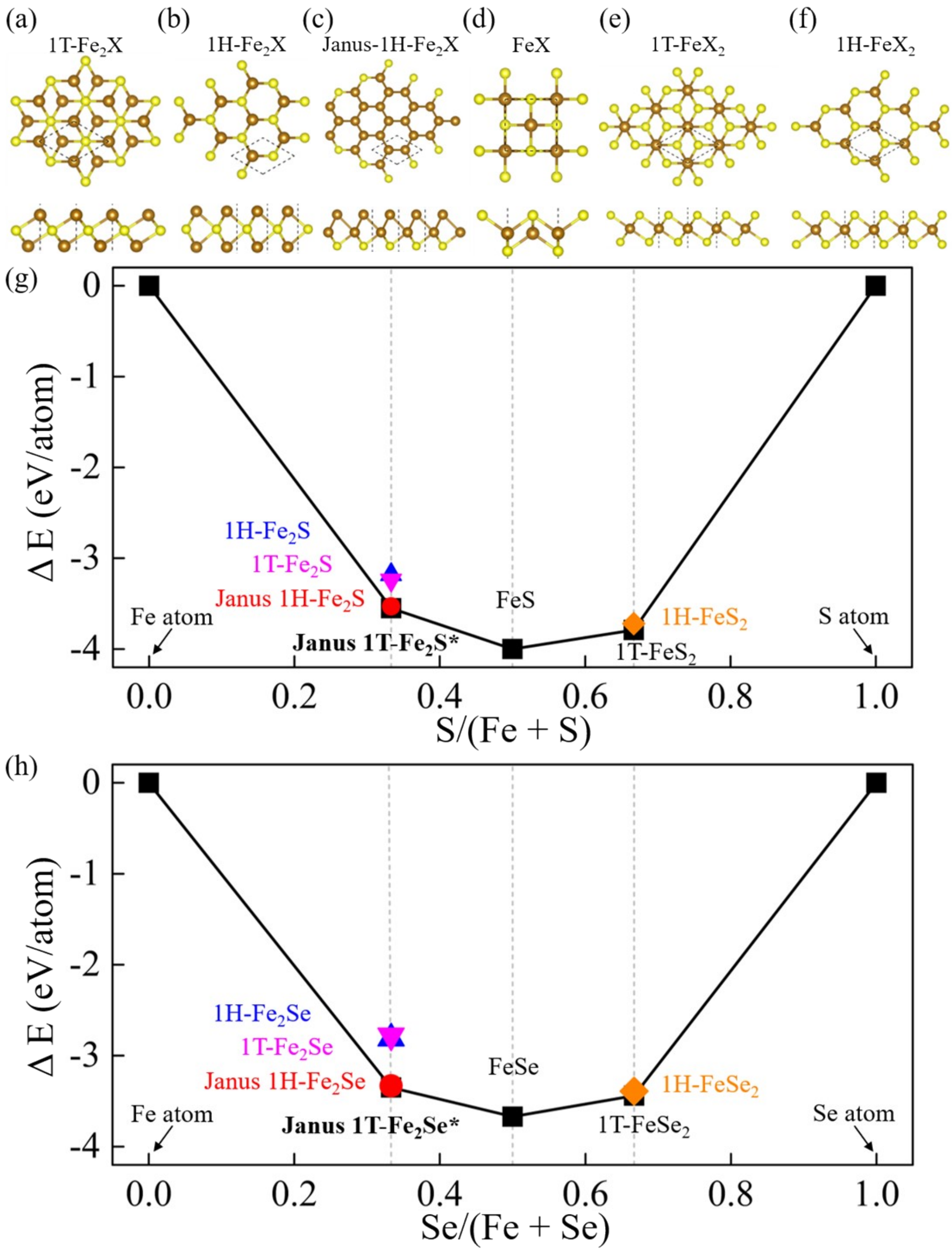

Figure S5. The top and side views of the competing phases and other Fe-X (X = S, Se) monolayers, including (a) 1T-Fe_2X, (b) 1H-Fe_2X, (c) Janus 1H-Fe_2X, (d) FeX, (e) 1T-FeX_2, (f) 1H-FeX_2. (g) Convex Hull data for Janus Fe_2S and (h) Fe_2Se monolayers with respect to the Fe, X atoms, competing phases and previously predicted stable geometries of FeX and 1T/1H-FeX_2 monolayers.[9,10]

Table S2. Elastic constants (C_{11}, C_{12}, in N/m), Young's modulus (N/m), and Poisson's ratio of the Janus Fe_2S and Fe_2Se monolayers.

	C_{11} (N/m)	C_{12} (N/m)	Y_{max} (N/m)	Y_{min} (N/m)	v_{max}	v_{min}
Fe_2S	36.67	35.38	2.53	2.53	0.97	0.97
Fe_2Se	41.22	27.35	23.06	23.06	0.66	0.66

Table S3. Relative energies (meV/f.u.) of the different magnetic configurations for the Janus Fe_2Se monolayer with respect to the FM ground state.

	FM	Néel-AFM	Stripy-AFM	Zigzag-AFM
Fe_2Se	0	494	304	275

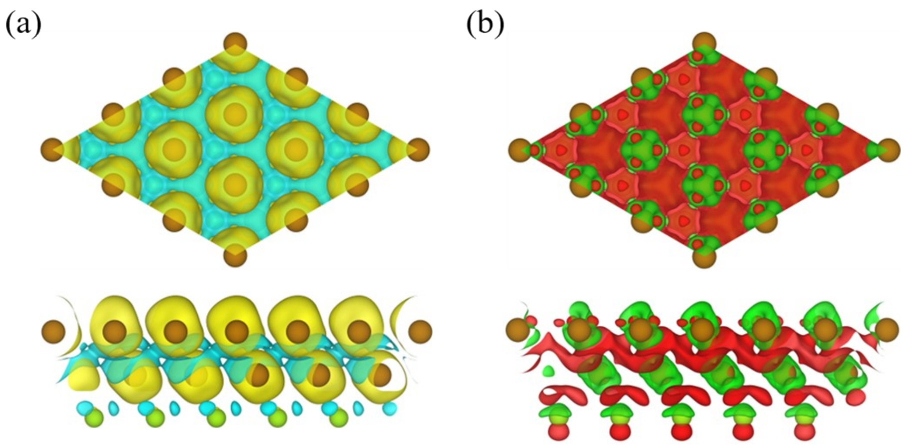

Figure S6. (a) Spin-polarized charge density and (b) differential charge density of the Janus Fe_2Se monolayer. The yellow and blue donate different spin states, respectively, and the red and green regions indicate charge accumulation and depletion, respectively.

Table S4. Bader charge of the Janus Fe_2X (X = S, Se) monolayers. The gain and loss of electrons are presented by negative and positive values, respectively. The unit for transfer charge is *e*.

	Fe_I	Fe_{II}	S/Se
Janus Fe_2S	0.002	0.412	-0.414
Janus Fe_2Se	0.001	0.311	-0.312

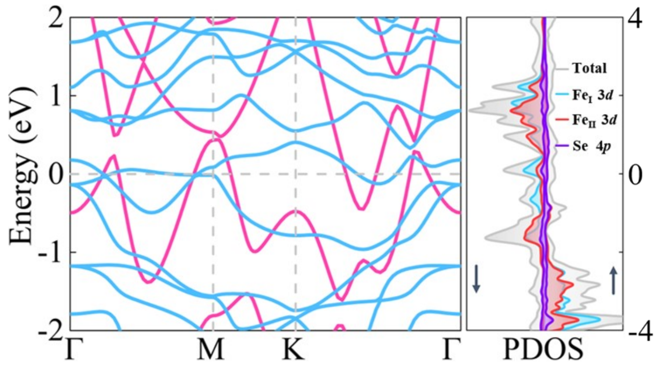

Figure S7. Spin-polarized electronic band structure and projected density of states of the Janus Fe_2Se monolayer. Red and blue lines represent the spin-up and spin-down channels, respectively. Fermi level is set to zero.

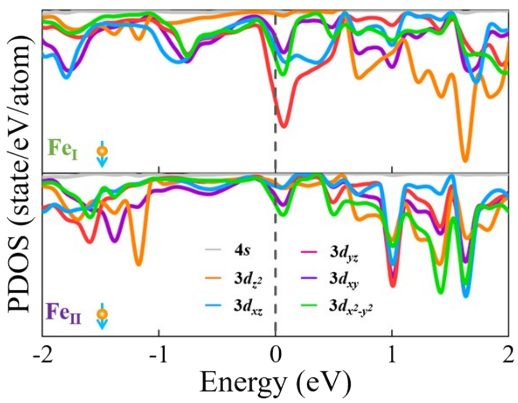

Figure S8. PDOS with spin-down state onto 4*s* orbital and five partial 3*d* orbitals of Fe_I and Fe_{II} atoms in Janus Fe_2S monolayer.

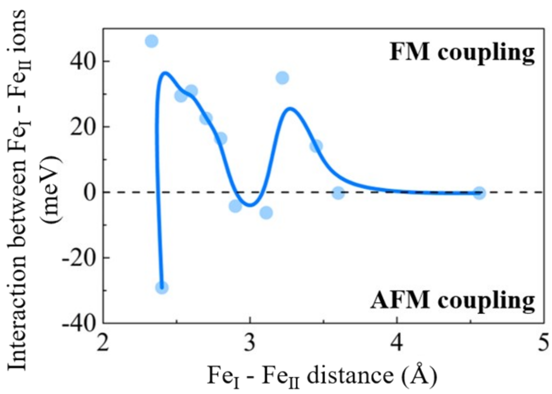

Figure S9. Calculated coupling interaction strength of interlayer Fe atoms as a function of Fe_I-Fe_{II} distance.

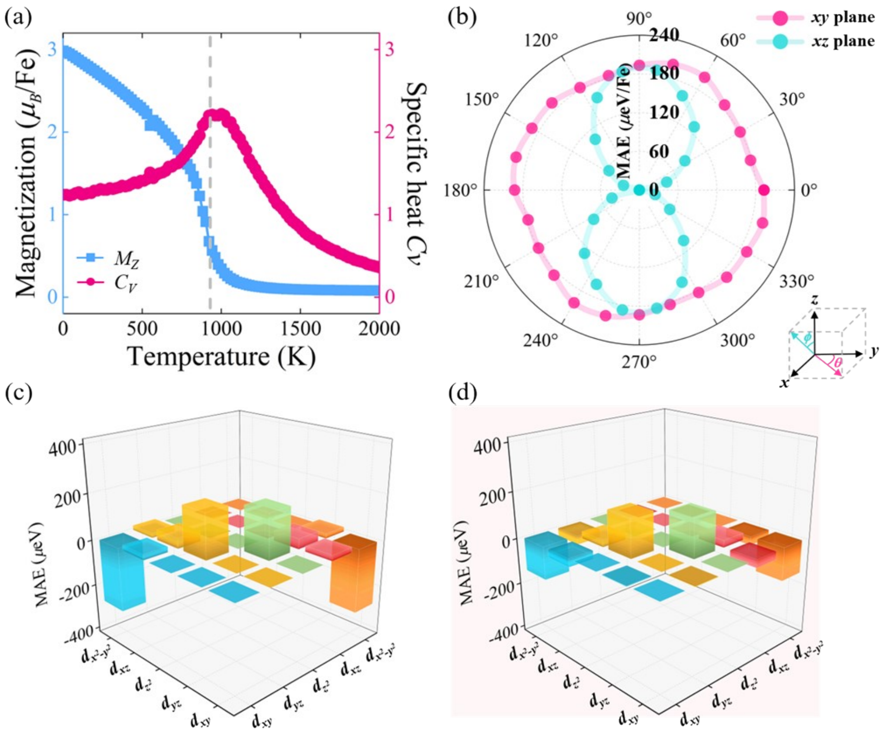

Figure S10. (a) Variation of the average magnetic moment (M_Z) of the Fe atom (blue) and the specific heat (C_V) (red) as a function of temperature obtained from Monte Carlo simulations based on the anisotropy Heisenberg model for the Janus Fe_2Se monolayer. (b) Angular-dependent MAE of the Janus Fe_2Se monolayer, where the pink and cyan indicate the magnetization in the *xy* and *xz* planes, respectively. Orbital-resolved MAE of the Fe atom with respect to the *d* orbitals for Janus (c) Fe_2S and (d) Fe_2Se monolayers.

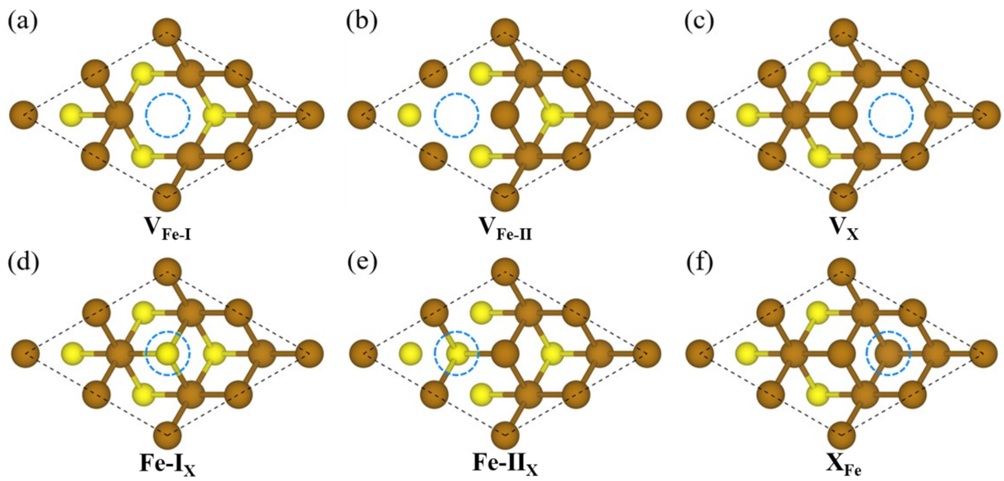

Figure S11. Atomic structures with the point defects in the Janus Fe_2X (X = S, Se) monolayers. The investigated defects belong to two classes, namely vacancy defects (e.g., (a) single Fe_I atom vacancy

($V_{Fe\text{-}I}$), (b) single Fe_{II} atom vacancy ($V_{Fe\text{-}II}$), and (c) single X atom vacancy (V_X)) and antisite defects (e.g., (d) a X atom substitutes a Fe_I atom (Fe-I_X), (e) a X atom substitutes a Fe_{II} atom (Fe-II_X), and (f) a Fe atom substitutes a X atom (X_{Fe})).

Table S5. Formation energy (E_{form}, eV) of the point defects of the Janus Fe_2X (X = S, Se) monolayers.

	$V_{Fe\text{-}I}$	$V_{Fe\text{-}II}$	V_X	Fe-I_X	Fe-II_X	X_{Fe}
Fe_2S	0.52	/	0.37	-1.85	/	0.72
Fe_2Se	0.58	1.31	-0.35	-2.04	/	0.59

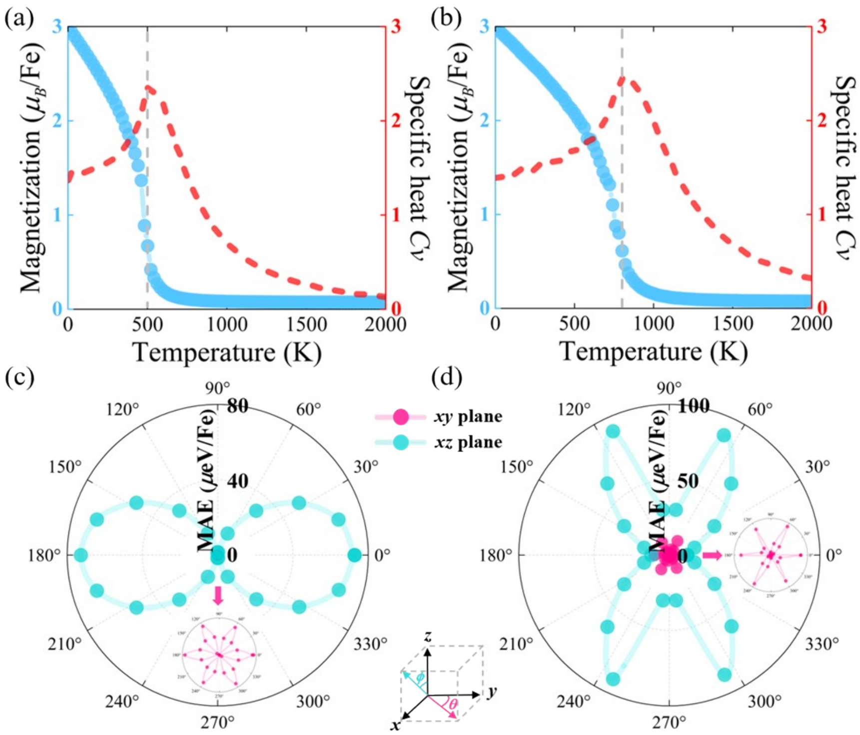

Figure S12. Variation of the average magnetic moment (M_Z) of the Fe atom and the specific heat (C_V) as a function of temperature obtained from Monte Carlo simulations based on the anisotropy Heisenberg model for the (a) Janus Fe_2S and (b) Fe_2Se monolayers with the Fe-I_X defect. Angular-dependent MAE of the (c) Janus Fe_2S and (d) Fe_2Se monolayers with the Fe-I_X defect.

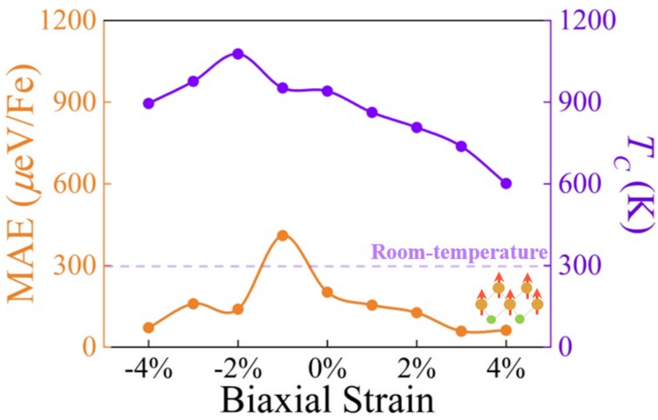

Figure S13. T_Cs and MAEs of the Janus Fe_2Se monolayer under different external biaxial strains.

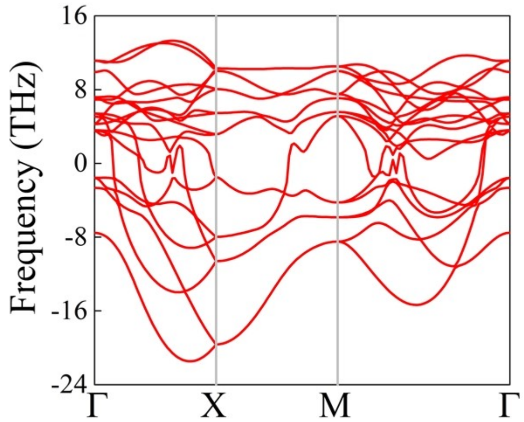

Figure S14. Phonon dispersive curves for the TS of Janus Fe_2S monolayer in ferroelastic transform process.

Table S6. Structural information of the predicted Janus Fe_2S and Fe_2Se monolayers.

	Space Group	Lattice Parameters (Å, °)	Atoms	Wyckoff Positions (fractional) *x*	*y*	*z*
		a= 2.8993	Fe (1a)	0.00000	0.00000	0.57236
Fe_2S	*P*3*m*1	*b*= 2.8993	Fe (1c)	0.66667	0.33333	0.50515
		γ= 120.00	S (1b)	0.33333	0.66667	0.44916
		a= 2.9721	Fe (1a)	0.00000	0.00000	0.56664
Fe_2Se	*P*3*m*1	*b*= 2.9721	Fe (1c)	0.66667	0.33333	0.50509
		γ= 120.00	Se (1b)	0.33333	0.66667	0.44458

References

1 Y. Wang, J. Lv, L. Zhu and Y. Ma, *Comput. Phys. Commun.*, 2012, **183**, 2063–2070.

2 Y. Wang, J. Lv, L. Zhu and Y. Ma, *Phys. Rev. B*, 2010, **82**, 94116.

3 G. Kresse and J. Furthmu, *Phys. Rev. B.*, 1996, **54**, 11169.

4 W. Kohn and L. J. Sham, *Phys. Rev.*, 1965, **140**, A1133–A1138.

5 J. P. Perdew, K. Burke and M. Ernzerhof, *Phys. Rev. Lett.*, 1996, **77**, 3865.

6 L. Liu, X. Ren, J. Xie, B. Cheng, W. Liu, T. An, H. Qin and J. Hu, *Appl. Surf. Sci.*, 2019, **480**, 300–307.

7 Y. Sun, Z. Zhuo, X. Wu and J. Yang, *Nano Lett.*, 2017, **17**, 2771–2777.

8 R. Kohlhaas, P. Dunner and P. N. Schmitz, *Z Angew Phys.*

9 C. Ataca, H. Şahin and S. Ciraci, *J. Phys. Chem. C*, 2012, **116**, 8983–8999.

10 A. Bafekry, I. Abdolhosseini Sarsari, M. Faraji, M. M. Fadlallah, H. R. Jappor, S. Karbasizadeh, V. Nguyen and M. Ghergherehchi, *Appl. Phys. Lett.*